Proceedings of
ASME TURBO EXPO 2001
June 4-7, 2001, New Orleans, USA

2001-GT-148

HEAT TRANSFER CHARACTERISTICS OF AN INTEGRATED COOLING CONFIGURATION FOR ULTRA-HIGH TEMPERATURE TURBINE BLADES : EXPERIMENTAL AND NUMERICAL INVESTIGATIONS

K. Funazaki, Y. Tarukawa and T. Kudo
Iwate University, Morioka, Japan

S. Matsuno and R. Imai
Industrial Machine & Plant Development Center
Ishikawajima-Harima Heavy Industries Co., Yokahama, Japan

S. Yamawaki
Aero-Engine and Space Operation
Ishikawajima-Harima Heavy Industries Co., Tokyo, Japan

ABSTRACT

This paper deals with fundamental research on heat transfer characteristics inside a cooling configuration designed for an ultra-high temperature turbine nozzle. The cooling configuration adopted in this study integrates impingement cooling and pin cooling devices into one body, aiming at the enhancement of the effective area for the impingement cooling. A large-scaled test model of this cooling system is constructed to measure its internal heat transfer distribution, where a number of pins are sandwiched between an impingement plate and a target plate. The target plate are provided with several air discharging holes. A focus of this study is on how the heat transfer characteristics depend on the effect of stand-off distance: a distance between these two plates. Ratios of the stand-off distance to the impingement hole diameter varies from 0.75 to 2.00. A transient measurement technique using narrow-banded thermochromatic liquid crystal (TLC) is employed to determine the heat transfer characteristics of the model. Numerical investigations using a commercial CFD code are also executed and those results are compared with the experimental data. It is accordingly found that the numerical results almost match the measurements. It is also shown that the addition of pins to the conventional impingement cooling system can produce about 50% increase in the effective cooling area.

INTRODUCTION

To meet the demand for higher TIT (Turbine Inlet Temperature) in aero-engines or gas-turbines with much less cooling air consumption, it is strongly needed to develop a revolutionarily new cooling system for high-pressure turbine stages. Several researchers examined their new turbine cooling technologies experimentally and numerically (Cho et al. [1], Glezer et al. [2], Uzol and Camci [3]). Impingement cooling has been frequently employed in turbine nozzle vanes because it easily attains much higher heat transfer coefficient than other internal cooling techniques. Ichimiya and Okuyama [4] studied a square array of four circular jets with a confining wall for various stand-off distances between a target plate and jet exit. Huang et al. [5] made detailed measurements on heat transfer distributions under an array of impinging jets, using transient measurement technique with thermochromatic liquid crystal (TLC). Gillespie et al. [6] examined heat transfer distributions in a model of an integrally cast cooling system aiming at the extended usage of impingement cooling to rotor blade applications. Having a target similar to that of Gillespie et al., Ekkad et al. [7] measured the impingement heat transfer on a target plate that contained film cooling holes. The authors also believe that further studies on the impingement cooling technology will provide us with promising ways to develop a new generation of turbine cooling system for future aero-engines.

This paper then describes some results from our fundamental researches on heat transfer characteristics inside of a cooling configuration designed for ultra-high temperature turbine nozzle. The cooling configuration of concern integrated impingement cooling and pin cooling devices into one body, aiming at the enlargement of the effective area for the impingement cooling. In addition, the enhancement of the heat transfer was also expected due to the interaction between the pins and the flow over the target plate on which the air from the impingement plate hit. A large scaled model of the system was constructed to measure the heat transfer on the surfaces of the target plate and pins. A stand-off distance, which is the distance between the impingement and the target plates, was equivalent to the pin height in the present case. Main focus was placed on the effect of stand-off distance upon the heat transfer characteristics on the internal surface of the test model. A transient measurement technique using thermochromatic liquid crystal (TLC) similar to that adopted by Huang et al. [5], which was modified by Funazaki et al. [8], was employed to determine the heat transfer characteristics of the model. Numerical investigations using a CFD code (CFX) with a low Reynolds number k-ε turbulence model were also executed. The purpose of the numerical investigation was two folds: one was to yield supplemental heat transfer and aerodynamic data for better understanding of the aero-thermal characteristics of the cooling system of concern. The other purpose was to examine to what extent recent CFD technologies could reproduce the flow field inside the complicated cooling system.

Nomenclature

c	: specific heat of the test model
c_{air}	: specific heat of the air
d	: diameter of impingement hole
H	: stand-off distance (spacing between the impingement and target plates), equivalent to the effective height of pin
h	: heat transfer coefficient
k	: thermal property (= $\rho c \lambda$)
N	: number of steps used for approximation
Nu	: Nusselt number (= hD/λ_{air})
Pr_t	: turbulence Prandtl number
q_w	: heat flux on the wall
R_p, R	: heat conductance with and without pin
Re	: Reynolds number (= $U_j d/\nu$)
T_g	: main flow temperature
T_i	: initial temperature of test model
T_w	: surface temperature
t	: elapsed time
U_j	: averaged jet velocity from the impingement hole
x,y,z	: coordinates
λ	: thermal conductivity of the test model
λ_{air}	: thermal conductivity of the air
ν	: kinematic viscosity
ν_t	: eddy viscosity
θ	: non-dimensional temperature
ρ	: density of the test model
ρ_{air}	: density of the air
τ_j	: delay time for j-th step

EXPERIMENTAL APPARATUS

Test Facility

Figure 1 shows the experimental setup used in this study. Inlet air temperature was controlled by a heater attached to the blower intake. The air flow rate was measured by the orifice. The test section was horizontally connected to the end of the main flow channel via a diffuser. The test section consisted of four acrylic-resin plates that formed square flow duct of 600 x 600 cross-section and the test model located at the end of the duct. The fan circulated the heated air inside the test section to minimize non-uniformity of the temperature in the duct caused by buoyancy. Four thermocouples, which were connected to a PC-controlled data logger via RS232C, acquired air temperatures of three vertically different positions at the upstream and one temperature at the downstream of the test model. The heated air was bypassed from the test section by the ball valve until the experiment started, with the air temperature being monitored by the thermometer at the exit of the bypass channel. The experiment began with switching the flow direction from the bypass channel side to the test section side. This operation was completed within half a second. The butterfly valve at the exit of the bypass channel adjusted the flow rate so that the flow rate did not change after the flow switching.

Test Model

Figure 2 shows three major components of the test model, which were an impingement plate, a target plate and pins. They were all made from acrylic-resin material. The shape of the impingement and target plates were 600 mm x 600 mm square with 15 mm thickness. The impingement plate had 15 impingement holes of 40 mm diameter, from which the heated air ejected towards the target plate. The target plate contained 10 air discharging holes of 40 mm diameter. The air discharging holes in the target plate were at the staggered positions with respect to the impingement holes in the impingement plate. These plates sandwiched the pins of 40 mm diameter. The effective pin height H, equivalent to the stand-off distance, was changeable from 30mm to 80mm, which provided non-dimensional stand-off distance H/d = 0.75, 1.00, 1.25, 1.50 and 2.00.

HEAT TRANSFER MEASUREMENT USING TLC

A brief explanation is given in the following on the transient technique for heat transfer measurement using thermochromatic liquid crystal (TLC). For more detail, see the paper published by Funazaki et al. [8].

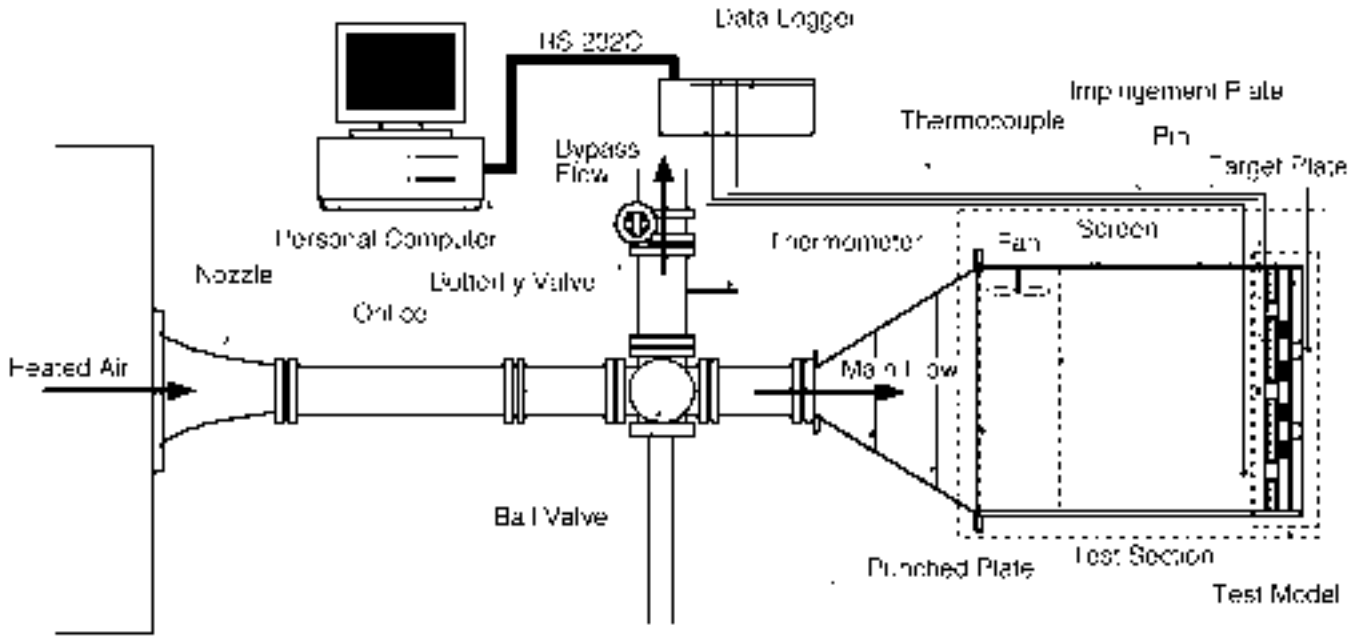

Figure 1 Test section including the test mode and the measurement system

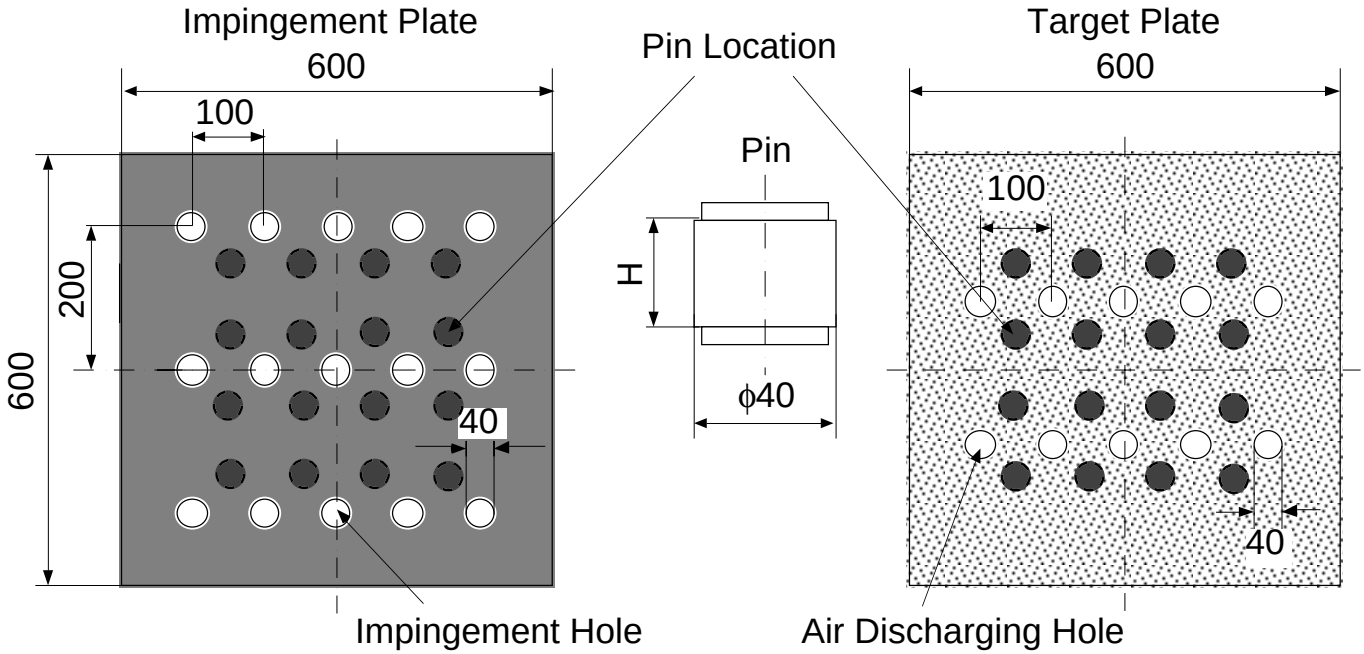

Figure 2 Test model consisting of an impingement plate, a target plate and pins

Suppose that a test model is suddenly heated by the flow over its surface with heat transfer coefficient h. Assuming one-dimensional heat conduction through the body, the surface temperature T_w at the elapsed time t can be calculated as follows:

$$\theta = \frac{T_w - T_i}{T_g - T_i} = 1 - \exp\left(\frac{h^2 t}{\rho c \lambda}\right)\mathrm{erfc}\left(\frac{h\sqrt{t}}{\sqrt{\rho c \lambda}}\right), \quad (1)$$

where θ is a non-dimensional expression of the surface temperature. However, since the flow temperature usually exhibit gradual change with time, some modification should be made on the above expressions. Application of Duhamel's theorem to this case yields the following equation for the surface temperature T_w,

$$T_w = T_i + \sum_{j=1}^{N} U\left(t - \tau_j\right)\left(T_{g,j} - T_i\right), \quad (2)$$

$$U\left(t - \tau_j\right) = 1 - \exp\left(\frac{h^2\left(t - \tau_j\right)}{\rho c \lambda}\right)\mathrm{erfc}\left(\frac{h\sqrt{t - \tau_j}}{\sqrt{\rho c \lambda}}\right), \quad (3)$$

where the rising curve of the actual flow temperature is approximated by a series of steps with constant temperature $T_{g,j}$ delayed by τ_j from the onset of the measurement. Taking a sufficient number of the steps in the approximation of the curve, T_w at an arbitrary elapsed time t can be uniquely determined by heat transfer coefficient h. This means that heat transfer coefficient at any point can be inversely obtained by numerically solving Eqs. (2) and (3) for given T_w and t. In the present study, TLC on the test model, which was recorded on VCR, provided information on the transient wall temperature T_w. Note that the temperature curve was divided into 40 steps, since it turned out that the resultant heat transfer coefficient h became almost unchanged over 40-step division.

Thermochromatic Liquid Crystal (TLC)

A narrow-band TLC was used in this study. Its temperature range over which one could identify color change was nominally from 32 °C to 34 °C. It was sprayed uniformly on the surfaces of the target plate and the fins as shown in Figure 3. TLC layer was coated directly on the target plate with the black coating sprayed on the TLC layer so that an observer could see the TLC color images on the target plate from the viewpoint A. On the other hand, black coating was first painted on the fin surface and TLC was sprayed on the black coating. In this case observations of the TLC on the pin surfaces were made from the viewpoint B.

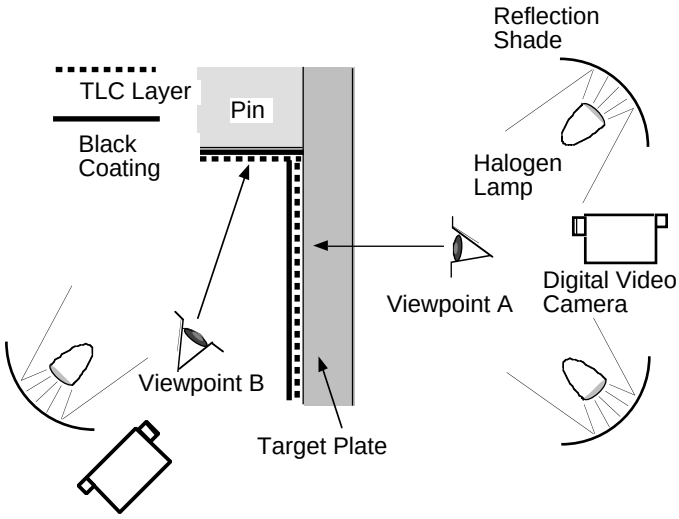

Figure 3 TLC layer and black coating over the test surfaces, also showing the viewpoints for the measurement and vedio cameras with the lighting

Image Capturing and Processing Two digital video cameras with 3 CCD recorded color images of the TLC simultaneously, one of which observed the TLC on the target plate and the other peered the TLC on the pins. Great care was paid to lighting of the TLC. Halogen lamps with low infrared emission were used for the lighting, with reflection umbrellas to scatter the light from the lamps. The positions of the

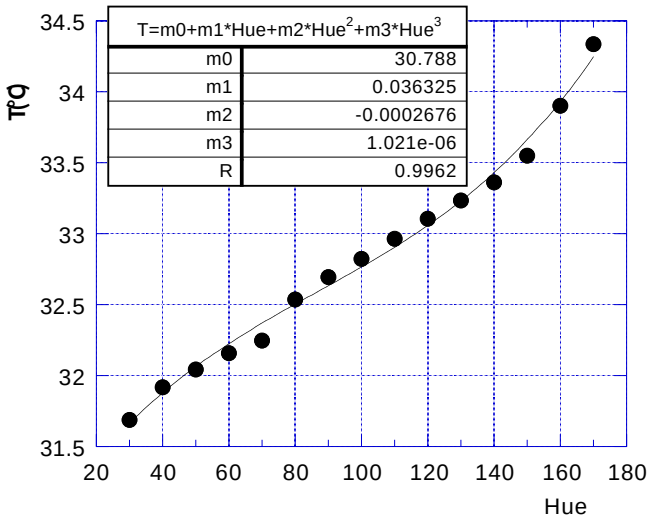

Figure 4 Relationship between Hue and temperature

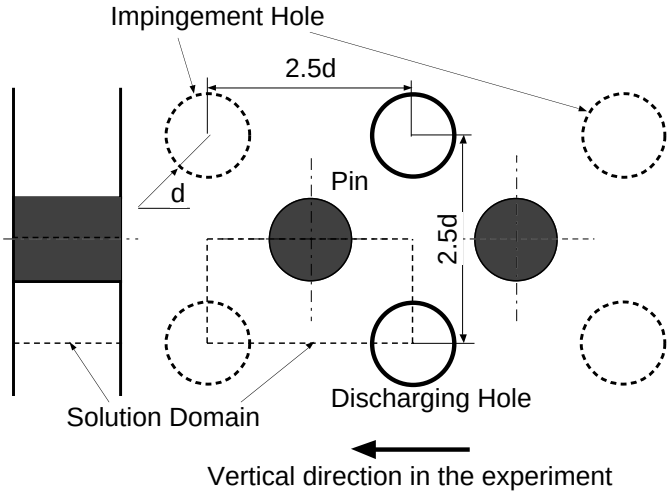

Figure 5 Solution domain

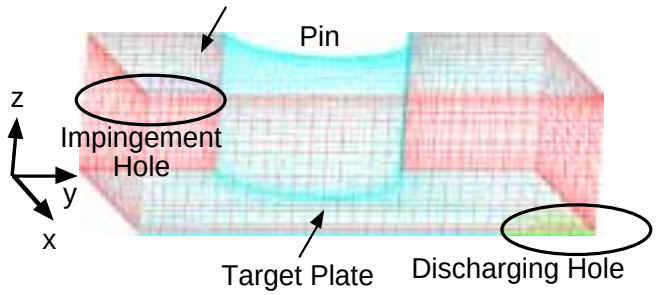

Figure 6 Grid system

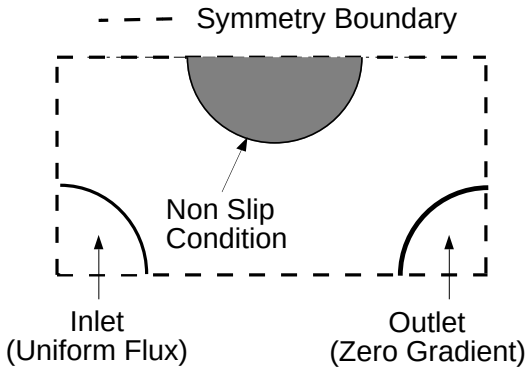

Figure 7 Specification of boundary conditions

cameras and the lamps against the test surface of concern were the same as those adopted in the calibration.

All the images of the TLC on the test surfaces were digitally recorded on the video tapes in NTSC format. After the measurement, these images were automatically transferred, captured and stored on a Power Macintosh equipped with FireWire (IEEE1394) ports via a DV cable, using a graphic software (Adobe Photoshop) with a plug-in software Photo-DV (Digital Origin Inc.). The captured image files, originally written in RGB color model, were then converted to files in HSL color model that contained three files of Hue, Saturation and Lightness with 8 bit resolution. As described later, the Hue value exhibited monotonous variation with the surface temperature over a certain temperature range. Therefore Hue data were used to determine the temperature distribution over the test surface of the model, although an additional usage of the other color information such as Saturation could contribute to improving accuracy in determining surface temperature. The files of Hue were finally transformed to ASCII files that could be read by Fortran-based program to determine the heat transfer distribution.

Calibration Calibrations were conducted using a calibration model to determine the relationship between the Hue value and the temperature (see Funazaki et al. [8]). The calibration model generated temperature gradient over an electrically heated stainless-steel tape on which the black coating and the TLC were sprayed in a similar manner with the test model. The above-mentioned image capturing system grabbed the color images on the calibration model, while thermocouples attached to the backside of the tape measured the temperature distribution along the tape. Figure 4 shows the relationship between the Hue value and temperature for the target plate measurement. A similar curve was also acquired for the pin surface measurement. Each of the relationships was approximated by a 3rd-order polynomial, which was implemented into the program code.

Uncertainty Analysis The calibration data revealed that an error of wall temperature ΔT_w given by the TLC was about ± 0.2 [K]. However, this was not the case for the temperature measurement on the pin because the pin surface was usually far from normal to the optical axis of the video camera. It was evident that the surface inclination angle to the camera axis incurred some ambiguity in Hue-temperature relationship, which could not be avoided especially for the pin surface observations. The previous study of Funazaki et al. [8] found that 50-deg surface inclination could change the temperature measured with the TLC by 0.45 [K]. Besides, errors of the main flow temperature and the initial temperature of the model were about ± 0.2 [K]. Taking these errors into account, it followed that the relative error of the measured heat transfer coefficient was about 6% for the target plate and more or less 10% for the pins.

Test Condition

Reynolds number of the present study Re, based on the impingement-hole diameter d and the averaged jet velocity from the hole U_j, was 1.0×10^4.

FLOW ANALYSES

Analysis Tool

The flow field inside the test model was numerically examined by use of a FVM-based CFD package, CFX Ver. 4.2 (AEA Technology), which solved Reynolds-averaged Navier-Stokes equations in conjunction with the continuity equation and the energy equation for incompressible flow. In consideration of the periodic flow field expected from the model configuration, the solution domain was specified as shown in Figure 5, which contained a half pin, a quarter impingement and discharging holes inside. As for the turbulence model, a low-Reynolds number $k-\varepsilon$ model proposed by Launder and Sharma [9] was used because Launder-Sharma $k-\varepsilon$ model reportedly provided reasonable prediction of heat transfer coefficients of impinging jets [10]. A BFC-type structured grid system was employed in this study. Figure 6 depicts an example of the grid systems adopted in the analysis for H/d = 0.75, where 17, 33 and 31 grid points are used in the x, y and z directions, respectively. A number of the grid points were clustered near the solid wall so that the closest grid point located under y^+ = 2.5, which resulted in good resolution of the wall-bounded shear flow analyses. For larger H/d cases, grid points along the z direction were accordingly increased from 31 up to 44 (for H/d = 2.00), keeping the grid density near the end walls the same as that of H/d = 0.75 case.

Boundary Conditions

Figure 7 gives the reader a brief idea on what kind of boundary conditions were used in the calculation. For the sake of simplicity, uniform mass flux condition was specified as an inflow condition from the impingement hole. Some experiences revealed that this simple approach worked well. For example, non-uniform mass flux condition that considered the boundary layer of 0.025 d thickness (1 mm) at the exit of the impingement hole changed averaged heat transfer coefficient only by less than 0.5%. Inlet turbulence kinetic energy k_{in} was set to be $0.01\,U_j^2$ and initial dissipation rate was $k_{in}^2/0.05d$. Zero-gradient condition was used for all flow variables at the outlet region. The boundaries surrounding the solution domain, designated by broken lines in Figure 6, were regarded as symmetry boundary. Non-slip condition was applied to the solid walls. Concerning the thermal condition, the inlet air temperature T_g was set to be 50 °C, while all wall temperatures were uniform and fixed to be 30 °C. Heat transfer coefficient h was then determined by the following equation,

$$h = q_w \big/ \left(T_g - T_w\right), \tag{4}$$

$$q_w = -\left(\lambda_{air} + \frac{c_{air}\rho_{air}\nu_t}{Pr_t}\right)\frac{dT}{dn}, \tag{5}$$

where dT/dn was an air-temperature gradient on the wall.

EXPERIMENTAL RESULTS

Heat Transfer Coefficients

General Features Figure 8 shows an example of the heat transfer distributions measured on the target plate for H/d = 1.0. In order to avoid the readers' misunderstanding, Figure 9 displays the locations of the impingement and discharging holes as well as the pins. Note that the heat transfer measurements on the pin surfaces were made using two pins inside the pin zone in Figure 9 because it was difficult to properly shed the light to other pins.

Although the heat transfer distribution in this figure was not symmetric with respect to the vertical and horizontal center lines of the plate, partially due to buoyancy or side wall effect of the test duct, there appeared several interesting features in the figure to be noted. As indicated by the circle A, high heat transfer regions of ring-like or

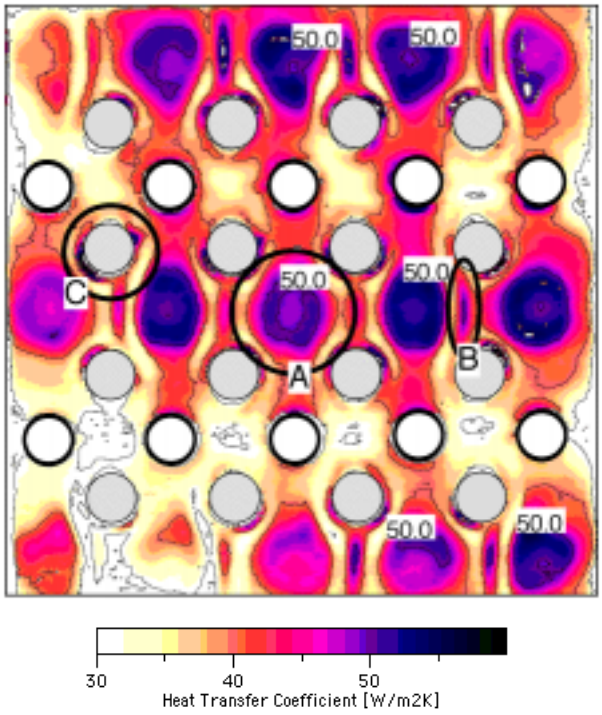

Figure 8 Heat transfer distribution on the target plate for H/d = 1.0

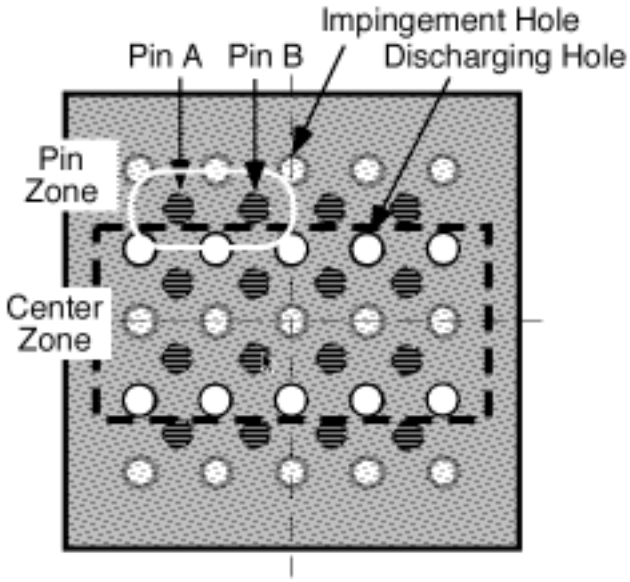

Figure 9 Locations of the holes and the pins with the identification of the zones to be examined

donut-like shape appeared where the air jets impinged on the target plate. In this case relatively low heat transfer regions emerged in the middle of the high heat transfer regions. This was because the jets still kept potential cores inside before they hit the target plate or the jets were at the early stage of their transition to turbulence. After the impingement, the jets tended to exit from the discharging holes, inducing high heat transfer on the area over which the air swept. One might also notice another high heat transfer regions of stripe-shape emerging between two neighboring jets impinging on the plate. These were probably induced by the interaction between the two wall jets originating from the two neighboring impingement jets. Some studies rel-

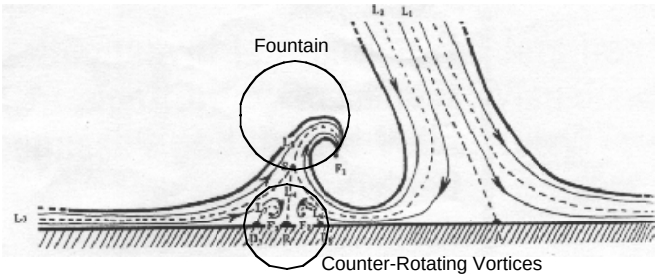

Figure 10 Fountain effect

evant to this finding was made by Bernard et al. [11] or Cho and Rhee [12]. They found that the jets rolled up and moved upward after the interaction as shown in Figure 10 and they called it a fountain effect. At the same time two counter-rotating vortices appeared under the 'fountain'. These vortices locally impinged on the plate, which could be attributed to the appearance of the stripe-shape high heat transfer regions. As will be given in the next section, the numerical calculation also verified the existence of the counter-rotating vortices. Near the junction between the pin and the target plate, high heat transfer regions marked with circle C came into view, which was due to horseshoe vortices.

In the following, discussions on the heat transfer distribution over the target plate surface are based on the data taken from the center zone of the target plate as shown in Figure 9.

Effects of Stand-Off Distance Figure 11 demonstrates the effect of the stand-off distance on the heat transfer over the target plate. A frame of broken line is shown in each of the contours to indicate the area where the experimental data are compared with the numerical results as shown in Figure 13. Although patterns of the three heat transfer distributions were similar with each other, relatively low heat transfer regions appearing at the center of the jets became obscure for larger stand-off distance case. For H/d = 2.00 the highest heat transfer occurred at the center of the impingement jets and heat transfer level of the stripe-shape regions between two neighboring jets slightly decreased in comparison with the other lower H/d cases. Figure 12 exhibits heat transfer distributions on the two pin surfaces for three stand-off distances. In this case the camera position were slightly changed for each of the test cases in order to prevent pin A (nearest pin to the camera) from blocking the view of the surface on pin B. Note that the heat transfer on pin A became lower than that on pin B, which corresponded to the appearance of the lower heat transfer coefficient on the left upper corner of the target plate as shown in Figure 8. In any cases the highest heat transfer regions occurred near the upper side of the pin-target plate junction. It seemed that some amount of the ejected air from the impingement hole flowed over the target plate like wall jet after the impingement on the target plate, then hitting the pin on the surface near the junction.

(a) H/d = 0.75

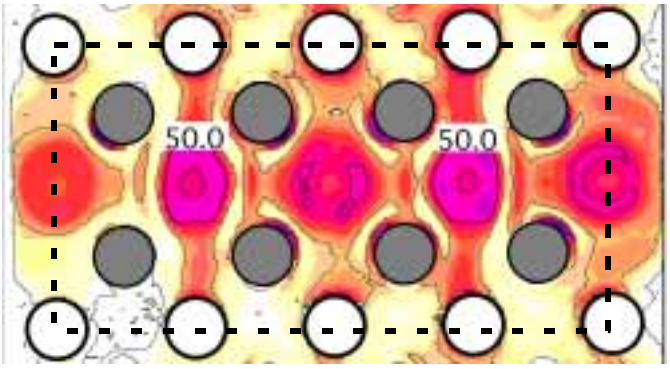

(b) H/d = 1.25

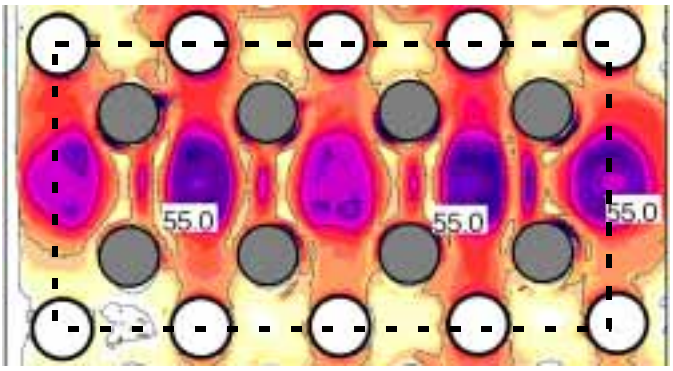

(c) H/d = 2.00

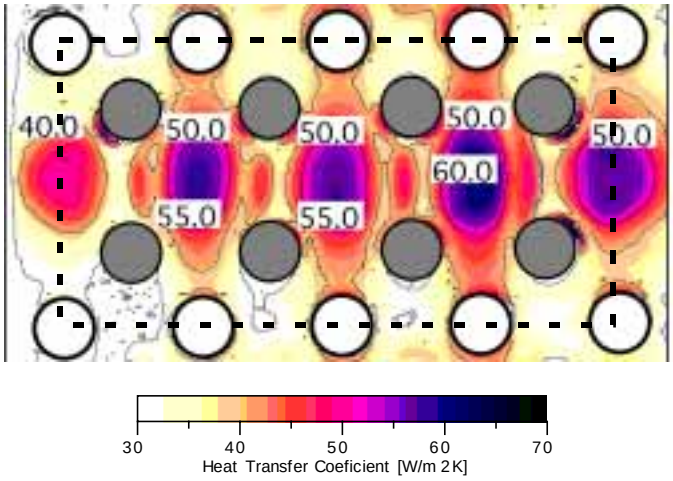

Figure 11 Effects of the stand-off distance on the heat transfer distribution over the target plate

NUMERICAL RESULTS

Local Heat Transfer Distributions

Figure 13 is numerical results of heat transfer distribution on the target plate obtained for three stand-off distances, H/d = 0.75, 1.25 and 2.00. Note that each of the heat transfer distributions was constructed from 8 identical numerical results obtained on the area as shown in Figure 7, taking advantage of the symmetry assumed in the calculation. Comparisons of these results with the experiment such as Figure 8 or Figure 11 show that the calculation successfully reproduced several features of the heat transfer distribution acquired from the experiments, such as a ring-like region of high heat transfer appearing at the location where the jet impinged on the target plate (circle A in Figure 8), the stripe-shaped region between two neighboring impingement jets (circle B in Figure 8) or a necklace-like region around the root section of the pin (circle C in Figure 8). The numerical calculation also captured the appearance of low heat transfer regions near the pins or between the jets. Furthermore, due to its high resolution, the calculation could provide more detailed information on the heat transfer distribution than the measurement could. For example, the necklace-like high heat transfer regions gradually became small or the above-mentioned low heat transfer regions tended to diminish for higher H/d. One can also identify locally high heat transfer regions near the edges of the discharging holes. A close inspection on the experimental data verified this finding.

(a) H/d = 0.75

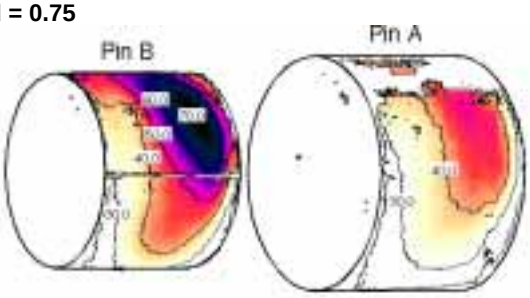

(b) H/d = 1.25

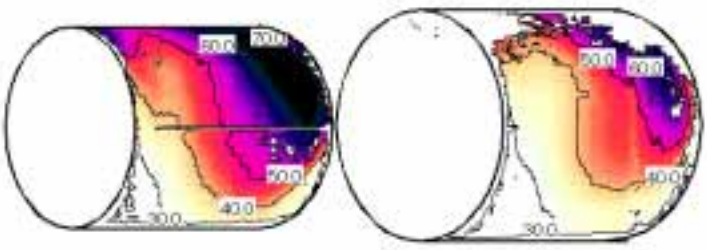

(c) H/d = 2.00

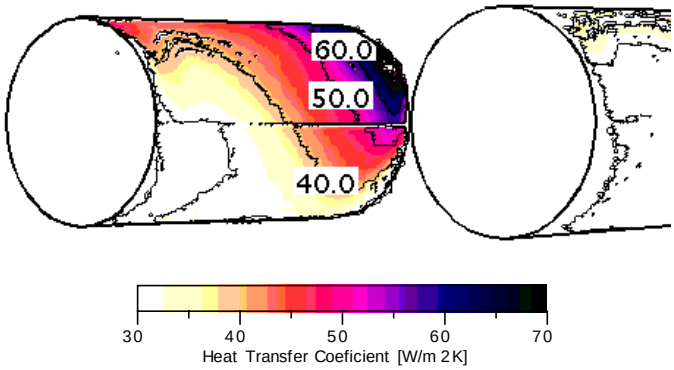

Figure 12 Effects of the stand-off distance on the heat transfer distribution over the pin surface

Figure 14 shows heat transfer distributions on the pin surface for the three stand-off distances likewise in Figure 13. By comparing these data with the experiments as shown in Figure 12 it follows that the calculated heat transfer distributions resembled those obtained by the experiments considerably, especially in terms of the appearance of maximum heat transfer coefficients near the root section of the pin. In addition, relatively high heat transfer regions over the pin surface tended to extend towards the impingement plate according to the increase in the stand-off distance, while such a extension seemed saturated at H/d = 1.25.

Aerodynamic Features

Figure 15 shows velocity vectors calculated for H/d = 0.75 on two cross sections of the flow field, i.e., A-A section and B-B section. As shown in the above of Figure 15, the A-A section was aligned with the centers of the impingement holes, and the B-B section included one impingement hole axis and one pin axis. From the velocity vectors on the A-A section one can see the interaction between two neighboring impingement jets on the target plate, which induced a 'fountain' movement at the collision point of the jets as seen in Figure 10, then accompanied by a large circulation between the impingement jet and the fountain. There appeared a reverse flow underneath the fountain on the target plate and this could be attributed to the emergence of the stripe-shaped high heat transfer region between the impingement jets. On the other hand, the velocity vectors on the B-B section revealed that the impingement jet behaved like wall jet after hitting the target plate. The wall jet headed for the pin almost in parallel with the target plate, maintaining high speed within a relatively narrow band compared to the wall jet appearing on the A-A section. The jet then impinged on the pin surface, resulting in the considerably high heat transfer region on the pin surface as seen in Figure 14. Near the junc-

(a) H/d = 0.75

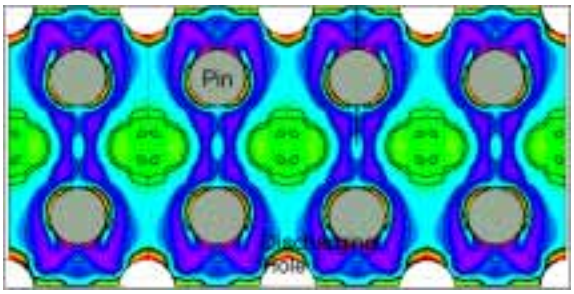

(c) H/d = 1.25

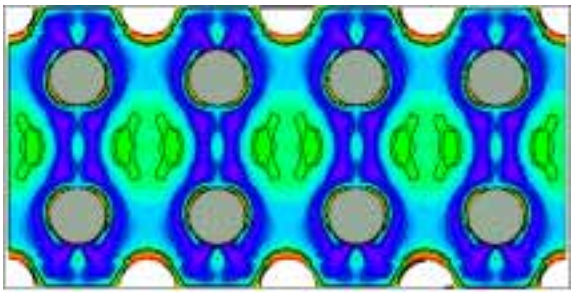

(c) H/d = 2.00

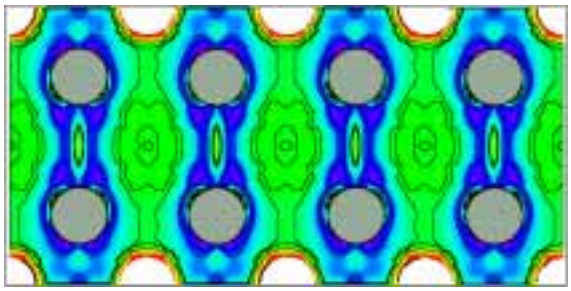

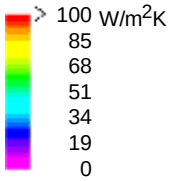

Figure 13 Numerical results of heat transfer distribution on the target plate for three stand-off distances

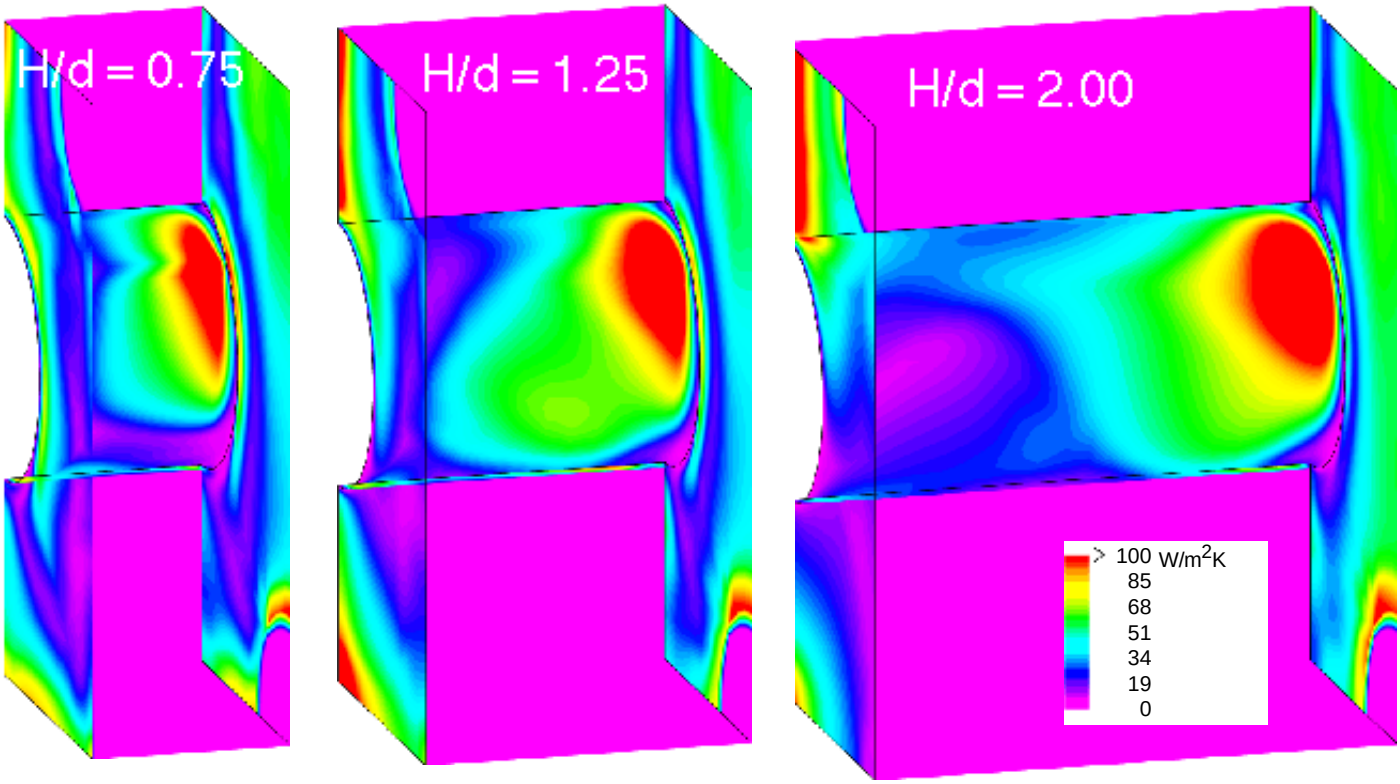

Figure 14 Numerical results of heat transfer distribution on the pin for three stand-off distances (left : H/d = 0.75, center : H/d = 1.25, right : H/d = 2.00)

tion between the pin and the target plate there also occurred a reverse flow, which corresponded to the appearance of a horse-shoe vortex around the foot of the pin. This reverse flow or horse-shoe vortex hit the pin-foot region on the target plate in a unsteady manner, causing the necklace-like high heat transfer regions there. In addition, it is worthy to note that the jet hitting the pin then moved upward along the pin surface up to about two-thirds of the pin height. A similar flow event was also observed in Figure 16 for the case of H/d = 1.25. It is evident that these upward flows along the pin promoted the expansion of the high heat transfer region towards the impingement plate, while for much larger H/d cases the effect of the upward flow tended to saturate.

DISCUSSIONS

Figure 17 shows averaged heat transfer coefficients on the target plate and the pin surface for all the non-dimensional stand-off distances obtained from the experiments and the calculations. The experimental heat transfer coefficients on the target plate and the pin surface exhibited their maxima between H/d = 1.25 and H/d = 1.5. Thereafter the averaged heat transfer on the pin decreased rapidly in comparison with that of the target plate. This was because the wetted area on the pin enlarged in proportion to the increase in the pin height, while the high heat transfer region near the target plate did not proportionally expand with the increase in H/d, as seen in the above. It should be noted that Ichimiya and Okuyama [4], through their experiments using four circular jets, found similar maxima of the average heat transfer coefficients around H/d = 1.5. Meanwhile, the numerical data exhibited reasonable agreement with the experiments, which indicates that the recent CFD technology has a good capability of predicting the heat transfer inside a cooling system with considerably complex geometry to a satisfying level from the engineering point of view. However, some discrepancies were also identified in Figure 17. In particular, the numerical heat transfer coefficient was still rising after H/d = 1.5, from which the experimental value started to decrease. It seems that the length of the potential core inside the impingement jet was slightly misestimated with the calculations, however, the true reason for this difference is not clear yet.

Lastly, the thermal performance of the present cooling system was examined in terms of the heat conductance, which is defined as effective area times heat transfer coefficient. In the present case the ratio of the heat conductance with the pins (R_p) to that without any pins (R) can be expressed as follows:

$$R_p/R = \frac{\tilde{A}\tilde{h}(H)}{Ah} = \frac{\left\{\left(A-\pi d^2/4\right)+\phi\pi dH\right\}\times\tilde{h}(H)}{Ah(H)} = \frac{\left\{\left((2.5d)^2-\pi d^2/4\right)+\phi\pi dH\right\}\times\tilde{h}(H)}{(2.5d)^2 h(H)} \quad , \qquad (3)$$

$$\phi = \tanh u_b/u_b \, , \quad u_b = \sqrt{\tilde{h}(H)(\pi d)\Big/\lambda\left(\pi d^2/4\right)} \qquad (4)$$

where $\tilde{h}(H)$ and $h(H)$ are average heat transfer coefficients for the cases with and without the pin and functions of the stand-off distance. From the experiments as well as the calculations it can be assumed that $\tilde{h}(H)$ = $h(H)$ and they are constant, which seems valid for $H/d \le 1.5$. According to this assumption the relative heat conductance R_p/R can be easily estimated and it varies from 1.22 for H/d = 0.75 to 1.45 for H/d = 1.5. This estimation is quite rough one, however it indicates that about 20% - 50% heat flux enhancement is possible by the application of the pin-type heat transfer promoters to a conven-

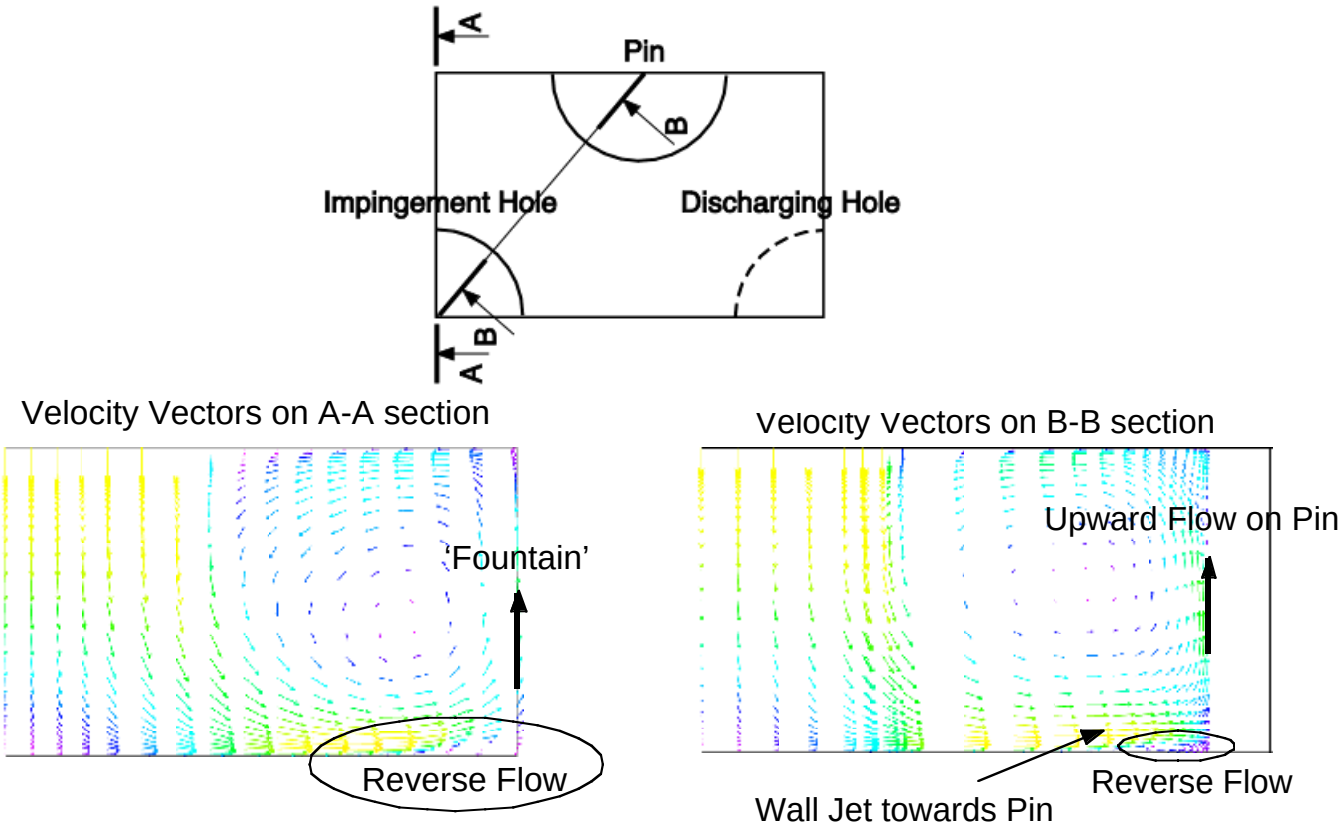

Figure 15 Calculated velocity vectors on two different planes(H/d = 0.75)

tional impingement cooling configuration. Although further studies on the details of the flow field and some modifications on the configuration are necessary, the authors believe that the cooling system investigated in this study or its derivative has a great potential to realize ultra-high temperature turbine nozzle vanes with less cooling air consumption.

CONCLUSIONS

This paper presented fundamental research on heat transfer characteristics inside a cooling configuration designed for ultra-high temperature turbine nozzle. A transient technique using thermochromatic liquid crystal (TLC) was employed to measure the heat transfer distributions on the target plate as well as on the pin surface for different stand-off distances. Also were made the numerical investigations to show to what extent a modern CFD code had a capability to predict the heat transfer inside the complicated cooling structure.

Important findings in this study are itemized as follows:

(1) The jets from the impingement plate induced high heat transfer on the target plate. In this case, since the target plate located very close to the impingement plate, ring-like regions of the high heat transfer appeared on the target plate.

(2) The two neighboring impingement jets collided at the midway of the jets, where another high heat transfer region emerged.

(3) The impinged jets also generate high heat transfer regions on the surfaces of the pins before being discharged from the cooling holes.

(4) Comparisons between the measurements and the calculations showed that the CFD successfully predicted the heat transfer inside the test model in terms of the local values as well as the area-averaged values for different stand-off distances.

(5) The rough estimation of the relative heat conductance attained in the present cooling system indicated that about about 50% heat flux enhancement was possible by the application of the pin-type heat transfer promoters to a conventional impingement cooling configuration.

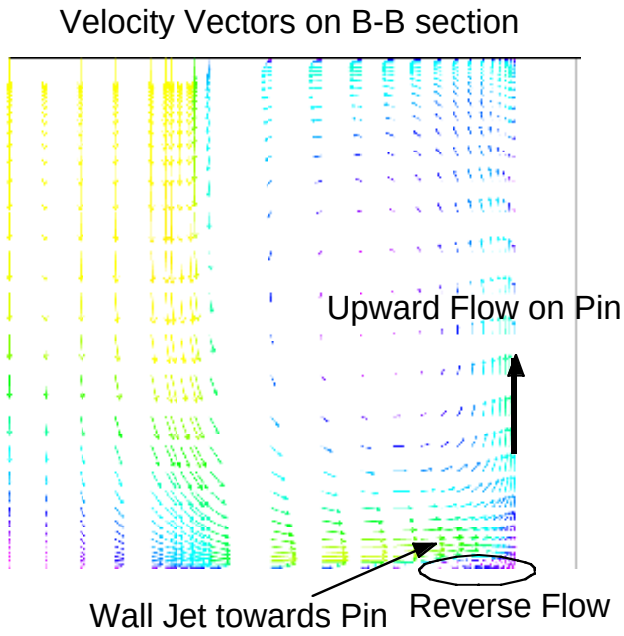

Figure 16 Velocity vectors on B-B section (H/d = 1.25)

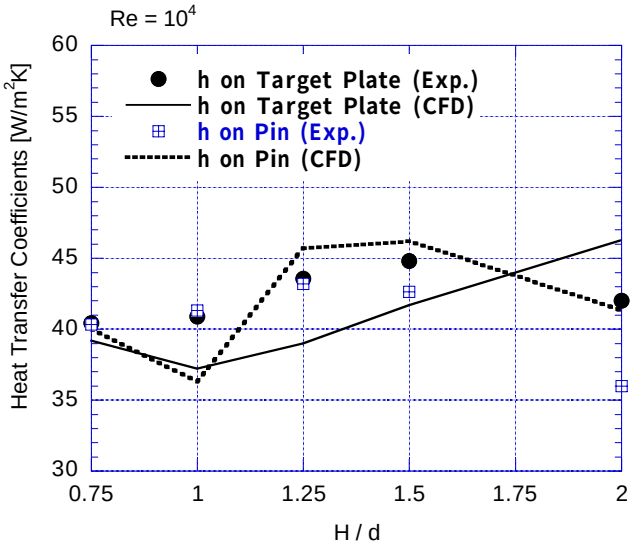

Figure 17 Comparisons between numerical and experimental averaged heat transfer coefficients

ACKNOWLEDGMENTS

The part of this work was conducted under the entrustment contract with NEDO (New Energy and Industrial Technology Development Organization) as a part of the National Research and Development Program (Industrial Science and Technology Frontier Program) of Agency of Industrial Science and Technology (AIST), Ministry of International Trade and Industry (MITI). The authors are greatly indebted to Mr. K. Ishizawa and Ms. N. Imamatsu, former students of Iwate University, for their contributions to the present study. The authors also acknowledge invaluable supports from Mr. F. Saito of Iwate University.

REFERENCES

1. Cho, H. H., Lee, C. H. and Kim, Y. S., 1998, “Characteristics of Heat Transfer in Impinging Jets by Control of Vortex Pairing,” ASME 98-GT-276.
2. Glezer, B., Moon, H. K., Kerrebrock, J., Bons, J. and Guenette, G., 1998, “Heat Transfer in a Rotating Radial Channel with Swirling Internal Flow,” ASME 98-GT-214.
3. Uzol, O. and Camci, C., 1998, “Oscillator Fin as a Novel Heat Transfer Augmentation Device for Gas Turbine Cooling Applications,” ASME 98-GT-150.
4. Ichimiya, K. and Okuyama, K., 1991, “Characteristics of Impingement Heat Transfer Caused by Circular Jets with Confined Wall,” Proceeding of Third International Symposium on Cold Regions Heat Transfer (Fairbanks), Vol. 1, pp. 523-532.
5. Huang, Y., Ekkad, S.V. and Han, J.C., 1998, “Detailed Heat Transfer Distributions under an Array of Orthogonal Impinging Jets,” Journal of Thermophysics and Heat Transfer, Vol. 12, pp. 73-78.
6. Gillespie, D. R. H., Wang, Z., Irlend, T. and Kohler, S. T., 1996, “Full Surface Local Heat Transfer Coefficient Measurements in a Model of an Integrally Cast Impingement Cooling Geometry,” ASME Paper 96-GT-200.
7. Ekkad, S.V., Huang, Y. and Han, J.C., 1999, “Impingement Heat Transfer on a Target Plate with Film Cooling Holes,” Journal of Thermophysics and Heat Transfer, Vol. 13, pp. 522-528.
8. Funazaki, K., Ishizawa, K. and Yamawaki, S., 1998, “Surface Heat Transfer Measurements of a Scaled Rib-Roughened Serpentine Cooling Passage by Use of a Transient Liquid Crystal Technique,” ASME 98-GT-515.
9. Launder, B.E. and Sharma, B.I., 1974, “Application of the Energy-Dissipation Model of Turbulence to the Calculation of Flow near a Spinning Disc,” Letter of Heat Mass Transfer, Vol. 1, pp. 131-138.
10. Shiravi, A.H., Mujumdar, A.S. and Kubes, G.J., 1995, “Numerical Study of Heat Transfer and Fliud Flow in Multiple Turbulent Impinging Jets,” Drying Technology, Vol. 13, pp. 1359-1375.
11. Bernard, A., Brizzi, L.-E. and Bousgarbies, J.-L., 1999, "Study of Several Jets Impinging on a Plate Wall: Visualizations and Laser Velocimetry Investigations," Trans. ASME Journal of Fluids Engineering, Vol. 121, pp. 808-812.
12. Cho, H. H., Rhee, D. H., “Local Heat/MAss Transfer Measurement on the Effusion Plate in Impingement/Effusion Cooling System,” ASME 2000-GT-252.